Optical properties of real photonic crystals: anomalous diffuse transmission

A. Femius Koenderink and Willem L. Vos

Complex Photonic Systems (COPS), MESA$^+$ Research Institute and Department of Science and Technology,
University of Twente, P.O. Box 217, 7500 AE Enschede, The Netherlands

Received August 20, 2004; accepted October 28, 2004; revised manuscript received November 23, 2004

Unavoidable structural disorder in photonic crystals causes multiple scattering of light, resulting in extinction of coherent beams and generation of diffuse light. We demonstrate experimentally that the diffusely transmitted intensity is distributed over exit angles in a strikingly non-Lambertian manner, depending strongly on frequency. The angular redistribution of diffuse light reveals both photonic gaps and the diffuse extrapolation length, as confirmed by a quantitative diffusion theory that includes photonic band structures. Total transmission corrected for internal reflection shows that extinction increases slower with frequency than Rayleigh's law predicts. Hence disorder affects the high-frequency photonic bandgap of fcc crystals less severely than expected previously. © 2005 Optical Society of America

OCIS codes: 050.1940, 160.4670, 260.1960, 260.3160, 290.1990, 290.4210.

1. INTRODUCTION

Since the original proposal in 1987,[1,2] it has been realized that photonic crystals hold a great promise both for optoelectronics and for basic physics. Photonic crystals are periodic dielectric composites with periodicities comparable to optical wavelengths causing the dispersion relations to become organized in band structures.[3] Optical Bragg diffraction is the fundamental mechanism determining the optical properties for such periodic dielectric media, yielding stop gaps for propagation in certain directions. Given a strong interaction between light and photonic crystals, a sufficiently modulated periodic potential is provided for photons to expect the optical analog of a semiconductor. Such a photonic bandgap, a frequency range for which no propagating photon modes exist, results in a vanishing density of states. A radically modified optical density of states is predicted to allow full control of spontaneous emission processes and to provide a solid-state environment for exciting (cavity) quantum electrodynamics. For device physics, photonic crystals promise novel emission sources, e.g., thresholdless lasers,[1,4] as well as components based on Bragg diffraction and strong dispersion such as ultrasmall waveguide structures[5] and superprisms.[6]

Recently, novel photonic crystals have been fabricated from materials with high dielectric constants for near-infrared and visible wavelengths by opal-based self-organization techniques or semiconductor nanofabrication methods (see Refs. 7 and 8 and references therein). These crystals interact so strongly with light that the propagation of light is inhibited for the majority of all directions.[9–11] Experiments have even shown that spontaneous emission from light sources embedded inside photonic crystals is strongly inhibited by a reduced density of states.[12,13]

As interference is at the basis of the photonic crystal properties, any mechanism that destroys the coherence of the composite structure can be detrimental to the promised advances. All real two- (2D) and three-dimensional (3D) structures inevitably suffer from disorder, as can be traced back to thermodynamical arguments.[14] Since optical experiments are usually interpreted in terms of photonic band structures, one might wonder how disorder influences the photonic band structures. This question is not meaningful, however, since band structures pertain to infinitely large crystals with perfect long-range order. Still, it is well known that faults modify the apparent stop bands probed by reflectivity, transmission, or internal light emission. In weakly photonic opals, Bertone *et al.* have observed broadened transmission stop bands as a result of finite size effects.[15] Vlasov *et al.* have observed additional Bragg conditions due to many stacking faults in their opals.[16] In similar systems, Astratov *et al.* found peculiar scattering peaks near stop band edges that were attributed to polycrystallinity.[17] Megens *et al.* have identified reduced attenuation in emission stop bands due to scattering from defects near the crystals' exit surface.[18] Furthermore, a large body of literature has shown that faults lead to large losses in waveguides incorporated in 2D crystal slabs.[3] The plethora of optical observations related to disorder invites the following basic questions: Is there a single optical gauge for disorder? How are optical properties affected in terms of such a gauge? And which type of structural disorder dominates the optical loss in general?

From electron transport in condensed-matter physics, it is known that disorder results in multiple scattering that is conveniently gauged by the so-called mean free path ℓ.[19] Optically, the mean free path is the characteristic length scale over which a coherent light beam is attenuated in the presence of optical disorder and also the scale characteristic of the propagation of diffuse light.[20,21] The mean free path has experimentally been determined for 3D photonic crystals on opals consisting of porous silica spheres[22,23] and on high-quality polystyrene opals and strongly interacting inverse opals.[24] Recently, a general theoretical model was developed to describe the mean free path for both 2D and 3D photonic crystals.[25] From a comparison with many experiments, it was inferred that size variations and displacements of the unit-cell building blocks are the dominant source of disorder. From the scaling of the mean free path with frequency, refractive-index variation, and structural size of the variations, it was concluded that large optical losses are an essential limiting factor to photonic crystal integrated circuits. Pioneering calculations have addressed the effect of size polydispersity and displacements on the photonic density of states[26,27] and on gaps in transmission[28] of fcc inverse opals. It was found that a combination of only 5% size variation and 5% displacement always results in a closing of the photonic gap.

In this paper we study the influence of disorder—gauged by the mean free path—on the optical properties of strongly interacting photonic crystals. We investigate the angle- and frequency-resolved characteristics of diffuse light transmitted by inverse opals. As photonic crystals ideally do not adsorb light, all light scattered out of an incoming Bloch wave will exit the sample after multiple random scattering events. Hence it is of prime importance to understand the properties of such unusual diffuse light. We demonstrate that the diffuse light is strongly affected by the photonic crystals, causing a drastic frequency-dependent redistribution of diffuse light over exit angles. We observe decreased diffuse intensity due to stop gaps, similar to Kossel lines. Unusual is the observation of strongly enhanced directional diffuse intensity, where light is pushed out of the crystal in the few remaining allowed directions.[29] We discuss how the redistribution, or "escape function," is quantitatively accounted for by extending diffusion theory to include internal reflections resulting from stop gaps in the photonic band structure. The non-Lambertian redistribution of light has important implications for studies of light that is emitted by sources embedded inside photonic crystals.[30,31]

Our experiments also reveal the frequency dependence of the angle-integrated or total transmission that bears information on the mean free path. Surprisingly, we find a decrease of the mean free path slower than Rayleigh's ω^4 law with frequency ω, as previously reported.[22] This points at the dominance of polydispersity, small displacements, and roughness as sources of random scattering, as opposed to missing spheres or grain boundaries.[25] We derive the angle-averaged reflectivity that sets the Milne extrapolation length for the diffusion process; contrary to usual diffuse media, these properties are strongly dispersive and reflect the photonic band structures. The paper is organized as follows: In Section 2 we review diffusion theory. In Section 3 we provide a description of our experiments. In Subsection 4.A we discuss the measured frequency dependence of the escape function at chosen detector angles, and in Subsection 4.B we present the angular redistribution of diffuse light at fixed frequencies. We extend the diffusion theory to photonic crystals with a model for the internal reflection coefficient $R_D(\omega;\mu_i)$ in Section 5. In Section 6 we present the total transmission measurements, and we use the extrapolation length ratio (see Section 5) to interpret the total transmission measurements in terms of the mean free path. Conclusions are presented in Section 7.

2. DIFFUSION THEORY

As a light beam with an intensity spectrum $I_0(\omega)$ strikes a photonic crystal surface (see Fig. 1), a fraction $R_{\text{front}}(\omega;\gamma)$ is (Bragg) reflected, depending on frequency ω and angle of incidence γ. We note that the effect of the mean free path on R_{front} is not discussed here and has been studied in Ref. 32. The remaining light that is not reflected propagates into the sample where it suffers from extinction due to scattering by defects. The light removed from the incident beam is multiply scattered on length scales equal to the transport mean free path ℓ.[33] For our high-quality opals and inverse opals the mean free path is of the order $\ell \approx 15\ \mu\text{m}$, as obtained from enhanced backscattering measurements.[24]

Since the thickness L of our crystals typically exceeds the mean free path, the crystals are opaque due to multiple scattering. In multiple-scattering media, the transport of multiply scattered light is usually well accounted for by the diffusion equation.[20,33] In this section we review results of diffusion theory that are relevant to diffuse transmission experiments on photonic crystals.

The success of diffusion theory depends on the use of appropriate boundary conditions, obtained by considering the diffuse fluxes at the sample walls. These conditions require that the diffuse intensity extrapolates to 0 at a distance z_e from the sample walls, where the extrapolation length

$$z_e(\omega) = \frac{2}{3}\left[\frac{1+\bar{R}_D(\omega)}{1-\bar{R}_D(\omega)}\right]\ell(\omega) \tag{1}$$

is determined by the polarization and angle-averaged reflectivity $\bar{R}_D(\omega)$ of the sample boundaries.[34–36] The extrapolation length is crucial to correctly determine ℓ from enhanced backscattering or total transmission measurements. For example, it is well known that the total diffuse

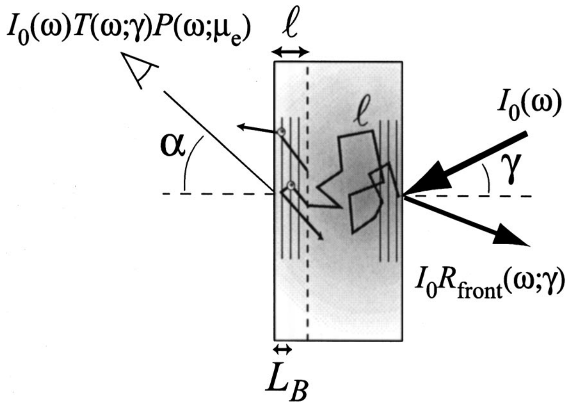

Fig. 1. As an incident light beam $I_0(\omega)$ impinges on a photonic crystal, a fraction $R_{\text{front}}(\omega;\gamma)$ is Bragg reflected, which depends on the frequency ω and the angle of incidence γ. In the sample the light diffuses with typical step length $\ell(\omega)$. The diffuse glow on the transmission side is measured as a function of $\cos\alpha = \mu_e$. The depth of stop gaps in the escape function is determined by ℓ and the Bragg attenuation length L_B (see Section 5).

transmitted intensity $I_T(\omega;\gamma)$ scales with the sample thickness according to

$$I_T(\omega;\gamma)=I_0(\omega)T(\omega;\gamma)=I_0(\omega)[1-R_{\mathrm{front}}(\omega;\gamma)]\frac{\ell(\omega)+z_e(\omega)}{L+2z_e(\omega)}. \tag{2}$$

Unless z_e is accurately known, ℓ can be determined only from the total diffuse transmission T if a series of measurements with fixed R_{front} is performed as a function of sample thickness L. For high-quality photonic crystals, varying L is a challenge, hence the extrapolation length should be known for a total transmission measurement to be useful to determine ℓ.

The extrapolation length ratio $\tau_e(\omega)=z_e(\omega)/\ell(\omega)$ can be determined from angle-resolved diffuse transmission (see Fig. 1), which is determined by refraction and reflection of the diffuse flux at the sample interface. According to diffusion theory, the probability for a diffuse photon in the sample to be transmitted at an external angle between $\alpha=\cos^{-1}\mu_e$ and $\cos^{-1}(\mu_e+\mathrm{d}\mu_e)$ from the surface normal satisfies[35,37]

$$P(\omega;\mu_e)\mathrm{d}\mu_e=\frac{3}{2}\mu_e[\tau_e(\omega)+\mu_i][1-R_D(\omega;\mu_i)]\mathrm{d}\mu_e. \tag{3}$$

Zhu and Durian *et al.*[35–37] have discussed the correct evaluation of the average reflectivity $\bar{R}_D(\omega)$ in Eq. (1) from the angle-dependent *internal* reflection coefficient $R_D(\omega;\mu_i)$. The angle-dependent internal reflection coefficient depends on the internal propagation angle $\cos^{-1}\mu_i$ and is assumed to be polarization averaged.

The result

$$\bar{R}_D(\omega)=\frac{3C_2(\omega)+2C_1(\omega)}{3C_2(\omega)-2C_1(\omega)+2}\quad\text{with}$$

$$C_n(\omega)=\int \mathrm{d}\mu\mu^n R_D(\omega;\mu),$$

obtained by an empirical flux argument, fixes the extrapolation length ratio according to Eq. (1). The proportionality constant 3/2 in Eq. (3) is set by the requirement that P is a properly normalized probability distribution. Since P describes the distribution of photons over the available escape angles, we refer to it as an escape function. The diffuse intensity transmitted at an angle between $\cos^{-1}\mu_e$ and $\cos^{-1}(\mu_e+\mathrm{d}\mu_e)$ factorizes in terms of the escape function and the total transmission as

$$I(\omega;\mu_e,\gamma)\mathrm{d}\mu_e=I_0(\omega)T(\omega;\gamma)P(\omega;\mu_e)\mathrm{d}\mu_e. \tag{4}$$

The angular dependence of the escape function P has been found to agree with experiments on random media if an effective refractive index is used to model $R_D(\omega;\mu_i)$ according to Fresnel diffraction and to convert internal to external propagation angles $\cos^{-1}\mu_i$ resp. $\cos^{-1}\mu_e$ by Snell's law.[35,36] As the refractive indices of random media such as powders or macroporous sponges are barely frequency dependent, only a weak frequency dependence of T, P, and ℓ occurs.[38,39] For highly dispersive photonic crystals, Snell's law does not describe the internal reflection coefficient well at all.[40] In contrast, light emanating from a depth $z<\ell$ from the crystal surface is Bragg attenuated (i.e., internally reflected) for angles and frequencies matching the Bragg condition, whereas it can leave the sample unobstructed for wave vectors away from the stop bands.[18,41] Hence the photonic band structure will give rise to a strongly angle- and frequency-dependent internal reflection coefficient $R_D(\omega;\mu)$, resulting in stop bands in the diffuse transmission. Furthermore, these stop bands cause a frequency-dependent extrapolation length.[24] The development and experimental verification of an internal reflection model relevant for photonic crystals is a central result of this paper.

3. EXPERIMENT

We have studied fcc photonic crystals consisting of air spheres in TiO_2 with a range of lattice parameters ($a=930,900,800,690,500\pm 20$ nm). Details of fabrication and characterization are reported in Ref. 42. The surfaces of the samples are parallel to the 111 crystal planes. At the blue edge of the L gap, corresponding to the first-order normal-incidence diffraction by 111 planes, more than 50% of the propagation directions are excluded,[9] attesting to the strong photonicity of the samples. Most of the structural disorder is inherited from the high-quality opal templates. As probed by small-angle x-ray scattering, both the size polydispersity and the rms displacements of the air spheres from the lattice sites are less than 2% of the sphere radius throughout the bulk of the crystals.[42] Together with the roughness of the titania shells [$\leqslant 10$ nm (Ref. 42)], this constitutes the main source of scattering determining the transport mean free path of $\ell\sim 15$ μm.[24] All small-angle x-ray Bragg spots observed match the fcc structure; we can place conservative upper bounds of much less than 10 vol. % on random stacking faults and <5 vol. % on the possible presence of the hexagonal close-packed structure, as found earlier.[43] The refractive index of the anatase TiO_2 backbone is found to be 2.7 ± 0.4, without recourse to a band-structure model. As the typical thickness $L\sim 200$ μm of the samples exceeds the mean free path, diffuse transport of light is indeed expected.

Samples were mounted on a rotation stage to control the orientation of the surface normal (parallel to the 111 reciprocal lattice vector) relative to the incident beam. As shown in Fig. 2, the detector was mounted on a rotation stage, allowing the detector angle α relative to the sample surface normal to be varied from 0° to 90°, independent of the incidence angle γ. Diffuse transmission spectra were recorded in the range $0°\leqslant\alpha\leqslant 90°$ every 5°. For spectrally resolved measurements, light from an incandescent lamp (tungsten–halogen) was passed through a Fourier-transform spectrometer (Biorad FTS-6000) operated at a resolution of 32 cm^{-1}. The beam emanating from the spectrometer was focused onto a pinhole, acting as a point source. This point source was imaged with a camera objective ($f=50$ mm) onto a spot of 0.40 mm radius encompassing many domains on the sample surface. The apex angle of the incident beam (10°) was designed to optimize the incident power. The angular resolution for diffuse transmission is set by the aperture of the detector of 5° and is independent of the apex angle of the incident beam. Angle-resolved measurements of the diffusely transmit-

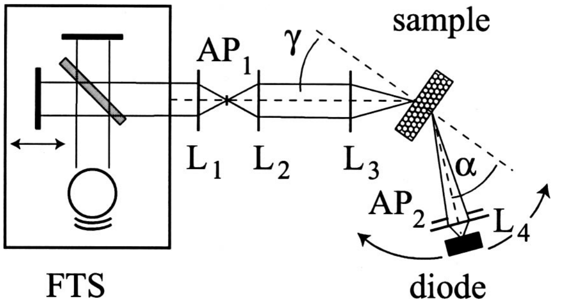

Fig. 2. Overview of the diffuse transmission setup. The output of a tungsten–halogen source is passed through a Fourier-transform spectrometer (FTS). The beam is focused onto a pinhole AP_1 by lens L_1. The pinhole acts as a point source that is imaged on the front sample surface by use of lens L_2 and camera objective L_3. The angle of incidence γ is controlled by rotating the sample. The detector angle α is changed independently by rotating the diode together with aperture AP_2 and lens L_4, which determine the angular acceptance.

ted intensity were obtained in the frequency range from 5500 to 14,000 cm^{-1} by use of both Si and InGaAs photodiodes. The diode signal yields an interferogram that is Fourier transformed to determine the diffusely transmitted intensity $I(\omega;\mu_e=\cos\alpha,\gamma)$. The total transmitted intensity spectra $I_T(\omega;\gamma)$ are determined by summing the angle-resolved diffusely transmitted intensity spectra weighted by $2\pi\sin\alpha\mathrm{d}\alpha$ to approximate the integration over a 2π solid angle. The total transmission $T(\omega;\gamma)$ is obtained by normalizing the total transmitted intensity spectrum $I_T(\omega;\gamma)$ to the lamp spectrum $I_0(\omega)$, measured by removing the sample from the setup. The escape functions $P(\omega;\mu_e=\cos\alpha)$ are determined by dividing the angle-resolved diffusely transmitted intensity spectra $I(\omega;\mu_e,\gamma)$ by the total transmitted intensity spectrum $I_T(\omega;\gamma)$ [see Eq. (4)]. Thus the escape functions are independent of the lamp spectrum.

Alternatively, a He–Ne ($\lambda=632$ nm) or Nd:YVO$_4$ ($\lambda=1064$ nm) laser beam could be used as single-frequency probes of the diffuse transmission, with a chopper and a lock-in amplifier. The laser beam path, not shown in Fig. 2, overlapped with the white-light beam path starting from lens L_1. The concomitant greater sensitivity allowed us to use cross-polarized detection, contrary to the white-light experiments. Cross-polarized detection avoids contributions of the unscattered beam to the detected signal.

4. ESCAPE FUNCTION MEASUREMENTS

A. Escape Function Versus Frequency at Selected Angles

Experimental escape functions $P(\omega;\mu_e)$ are shown in Fig. 3 for a sample with lattice parameter $a=930$ nm as a function of frequency ω for a large range of detector angles $\alpha(=\cos^{-1}\mu_e)$. The data set presented in Fig. 3 was obtained in a single run with incidence angle $\gamma=0°$. It should be noted that no scaling constants are involved in Fig. 3. We do not find a dependence of the escape function on the incidence angle γ for $0°\leqslant\gamma\leqslant 30°$. This result validates the factorization in Eq. (4), as it shows that $P(\omega;\mu_e)=I(\omega;\mu_e,\gamma)/I_T(\omega;\gamma)$ is independent of γ. This result can be understood from the diffusive nature of the samples; as the direction of propagation is fully randomized, the probability for a photon to leave the sample at a specific exit angle α is independent on the incidence geometry. The only effect of the incidence angle γ is due to the reflectivity of the front surface [R_{front} in Eq. (2)], which reduces the total transmission $T(\omega;\gamma)$ for frequencies and incident angles matching the Bragg condition (see Section 6).

At low frequencies $\lesssim 6700$ cm^{-1} the escape function is unaffected by internal reflection and typical for a random medium with $z_e\approx 2/3\ell$. As evident in Fig. 3, the escape function at an exit angle of $\alpha=15°$ is significantly reduced by $\sim$70% in a stop band centered at $\sim$8200 cm^{-1} with a FWHM $\sim$1000 cm^{-1}. This stop band in the escape function occurs because of internal Bragg reflections through the term $[1-R_D(\omega;\mu)]$ in Eq. (3) and moves to higher frequencies with increasing exit angle α. At angles α exceeding $\sim$35°, a much wider gap is evident in Fig. 3. Similar broadening and the occurrence of a double-peak structure have been observed in reflectivity experiments[44,45] and luminescence experiments[41] and have been explained in terms of a multiple Bragg wave coupling involving both 111 and 200 reciprocal lattice vectors.[44] Figure 3 shows that the stop band at these larger angles is preceded by a frequency range (8000–10,000 cm^{-1}) characterized by an increase of the escape function. This frequency range is coincident with the stop band at small detector angles. The increase has the same origin as the enhanced escape probability in the frequency range 9000–12,000 cm^{-1} evident in the escape function spectrum at small detector angles. As escape directions within a stop gap are blocked by internal Bragg reflection, photons are more likely to escape in the remaining directions, giving rise to an *enhanced* escape probability in directions not *coincident* with a stop gap. Equivalently, this enhanced escape probability can be interpreted as an increase of the extrapolation length because of a larger average internal reflection coefficient $\bar{R}_D(\omega)$.

Similar results were obtained for a multitude of samples with different lattice parameters (a

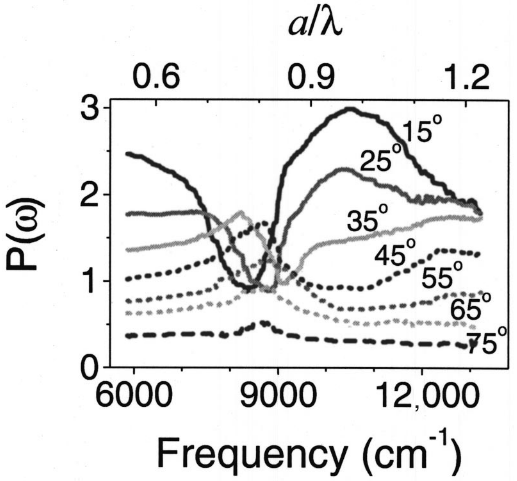

Fig. 3. Photon escape function as a function of frequency for an inverse opal with lattice parameter $a=930$ nm for exit angles $\alpha=15°,25°,35°,45°,55°,65°,75°$. The incidence angle is $\gamma=0°$. The top axis shows normalized frequency units a/λ where λ is the wavelength in vacuum. No relative scaling or offset was applied to the curves.

=930,900,800 nm). The shift along the frequency axis of the escape functions with lattice parameter confirms the photonic origin of the redistribution of the diffuse intensity. In conclusion, Fig. 3 clearly shows that the diffuse intensity possesses a pronounced angle- and frequency-dependent structure due to the strongly interacting photonic crystal. This point is particularly important in the interpretation of widely performed reflectivity or transmission experiments[7,8]: The commonly applied correction for a diffuse contribution to the signal by assuming a frequency-independent background, or even a Rayleigh-like diffuse scattering contribution,[22] is clearly incorrect. Instead, a correct interpretation rests on the interpretation by means of the escape function. In this respect a transmission measurement can be particularly misleading. Even if scattering by disorder precludes any coherent transmission (i.e., for thick samples $L/\ell \gtrsim 5$), a detector along the incoming direction will still register a (diffuse) spectrum with an attenuation band coincident with the photonic stop gap. Evidently a stop gap in transmission can be trusted only if the transmission for frequencies just *outside* the stop gap is close to 100%, indicative of low scattering. This requires an absolute calibration of the transmission.

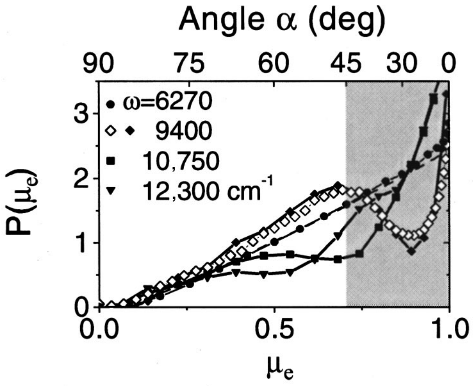

Fig. 4. Photon escape function as a function of the cosine μ_e of the escape angle α for an inverse opal with lattice parameter $a=930$ nm for frequencies $\omega=6270,9400,10{,}750,12{,}300$ cm^{-1} (filled circles, diamonds, squares, triangles, respectively) as extracted from a white-lamp data set. These frequencies correspond to $a/\lambda=0.58$, 0.87, 1.0, and 1.14. Open diamonds show a measurement obtained from the same sample with a Nd:YVO laser beam ($\omega=9400$ cm^{-1}). An angular scale is shown on the top axis. The shaded region corresponds to half of the range of the exit angle α relative to the surface normal. The dashed curve partially obscured by filled circles corresponds to calibration measurements on a dilute colloidal suspension.

B. Strongly Non-Lambertian Redistribution

The redistribution of diffuse intensity over exit angles can be more fully appreciated by considering the escape function as a function of angle for selected constant frequencies (see Fig. 4). The horizontal scale in terms of μ represents the large contribution of large exit angles in the distribution of intensity over the available hemisphere of exit directions. For clarity the exit angle range from 0° to 45° covering half of the available polar exit angle range is indicated in gray. As a calibration sample, we studied a vial filled with a dilute suspension of polystyrene spheres in water (dashed curve in Fig. 4). In accordance with Refs. 36 and 37, we find nearly Lambertian behavior, defined as $P(\mu_e)=2\mu_e$. Detailed analysis shows that the escape function of the calibration sample is accurately modeled by Eq. (3). A Fresnel-type model for the internal reflection coefficient was used, assuming an effective index of 1.33 typical of water and taking multiple reflections in the vial walls into account.[36]

For frequencies below the L gap ($\omega=6270$ cm^{-1}), the escape function of an inverse opal with $a=930$ nm closely resembles the escape function measured for the calibration sample, as shown by Fig. 4. From a fit of diffusion theory with a Fresnel model for the internal reflection coefficient, we estimate an effective refractive index of $n_{\mathrm{eff}}=1.27\pm0.15$. This effective index is consistent with a 10–20% volume fraction of solid material, depending on whether the effective index is assumed to correspond to the volume-averaged dielectric constant or volume-averaged refractive index, respectively. The nearly Lambertian distributions for low frequencies should be contrasted to the angular distribution of emitted photons for a frequency of 9400 cm^{-1} to the blue of the L gap. As demonstrated in Fig. 4, the escape function at this frequency is clearly reduced in the range from $\alpha=10°$ to 40° and enhanced both for near-normal exit angles and for exit angles exceeding 40°. These features, as extracted from the white-light experiment, are quantitatively reproduced in an additional single-frequency measurement with a Nd:YVO$_4$ laser beam ($\lambda=1.06$ μm), also shown in Fig. 4. If the diffuse intensity would be projected on a screen, this would correspond to a dark ring, with an apex angle centered at $\alpha=25°$. Because of the strongly photonic nature of the titania inverse opals, however, this dark ring has a very large angular width. With an increase in frequency, the dark ring grows in radius, shifting to a larger angle in Fig. 4. As an increasing fraction of solid angle is contained in the photonic stop gaps, the escape function at a near-normal exit angle is increased to more than 1.5 times the low-frequency value, resulting in a bright circle contained in the dark ring.

For the larger frequencies comparable to the stop band at angles exceeding 30°, a measurement on single-crystal samples would show an azimuthal dependence of the escape function since the 200 family of reciprocal lattice vectors oblique to the sample surface is involved in the Bragg diffraction. This dependence is lost in our experiments since our samples are polycrystalline. For weakly photonic colloidal crystals, narrow Kossel lines in the diffuse transmission have indeed been observed to show this azimuthal dependence.[46–48] For angles away from the Kossel lines, the angular-resolved diffuse transmission of such weakly photonic samples closely follows a Lambertian profile since the extrapolation length is barely affected by the narrow internal reflection lines. In contrast the dark rings shown in Fig. 4 extend over ~50% of the 2π-sr solid angle, and the geometry of the internal reflection is strongly affected by multiple Bragg wave coupling. The full band structure should therefore be used to interpret the features in the escape function instead of a geometric analysis with the free-photon dispersion appropriate for weakly interacting photonic crystals. Furthermore, the large angular extent of the features in the escape function causes the distribution of diffuse intensity to differ significantly from Lambertian for the full range of exit directions simultaneously. Hence, strongly interacting photonic crystals may provide a route to make strongly directional diffuse light sources, as proposed in Refs. 29 and 31.

5. DIFFUSE INTERNAL REFLECTION MODEL

The full data set to which Fig. 3 corresponds is presented as a contour plot in Fig. 5(a). For angles below ~40°, the shift of the stop band to a higher frequency with increasing exit angle is clearly discerned, as well as the broadening of the stop band for larger exit angles due to multiple Bragg wave coupling.[44] The concomitant enhancement of the escape function is evident in the range 9000–12,000 cm^{-1} for small angles $\alpha < 30°$ and in the range 7500–9000 cm^{-1} for large exit angles $30° < \alpha < 60°$. Here we proceed with a quantitative description of the data in terms of a theory that extends diffusion theory [Eq. (3)] to photonic crystals by using a model derived from a band-structure calculation for the internal reflection coefficient $R_D(\omega;\mu)$.

A. Internal Reflection Coefficient

The internal reflection coefficient of the inverse opals is semiempirically modeled as the sum of two Gaussian reflection peaks,

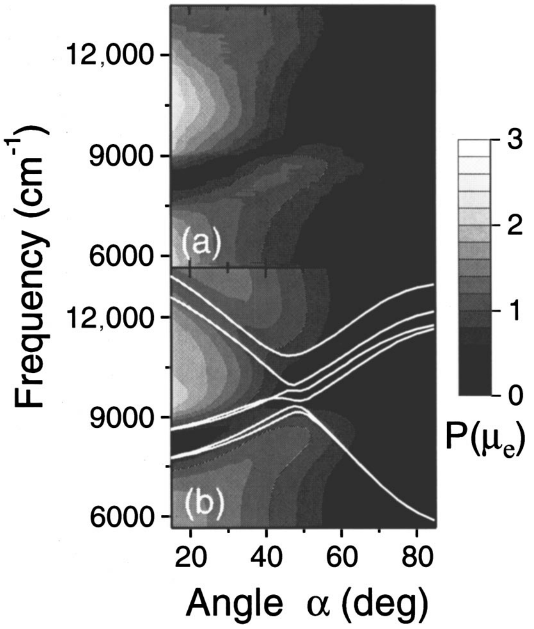

Fig. 5. (a) Contour plot of the measured photon escape function as a function of exit angle α and the optical frequency corresponding to an inverse opal with $a = 930$ nm. Right-hand panel (b): contour plot of the fitted escape function, according to the diffusion model [Eq. (3)] combined with an internal reflection coefficient derived from the band structure [Eq. (5)]. The lowest six bands along the LU direction are plotted in white; we used the effective index to transform the internal propagation angles into external propagation angles. The band structure alone can not fully explain the frequency and angle dependence of the escape function. A common gray scale is displayed on the right.

$$R_D(\omega;\mu_i) = R_1(\mu_i)\exp\left\{-\frac{[\omega-\omega_1(\mu_i)]^2}{2\Delta\omega_1(\mu_i)^2}\right\} + R_2(\mu_i)\exp\left\{-\frac{[\omega-\omega_2(\mu_i)]^2}{2\Delta\omega_2(\mu_i)^2}\right\}, \quad (5)$$

with angle-dependent peak reflectivities $R_{1,2}(\mu)$ and widths $\Delta\omega_{1,2}$. We expect such a model to capture the essential frequency dependence including the double-peak reflectivity features[41,44] if the center frequencies $\omega_{1,2}(\mu)$ are chosen consistent with the photonic band structure.

We calculated the band structure for a model of the titania inverse opals consisting of close-packed air spheres (radius $r = 1/4\sqrt{2}a$) on a fcc lattice surrounded by high-index ($\epsilon = 6.5$) spherical shells with outer radius $1.09r$, connected by cylindrical windows of radius $0.4r$. The window size and the volume fraction of solid material are in agreement with structural data,[42] and the resulting band structure has been found to agree with reflectivity bands in the frequency range of both the first and the second Bragg diffraction order.[44,49] Previously, it has been observed that the band structure along the LU line in reciprocal space (extended outside the first Brillouin zone) satisfactorily describes the angle-dependent reflectivity of polycrystalline samples.[44] Therefore we calculated the dispersion relation along the LU line and determined $\omega_1(\mu)$ and $\omega_2(\mu)$ from the calculated stop band edges. To convert the internal to external propagation angle, we used Snell's law with the average refractive index. Contrary to the fixed reflection band center frequencies $\omega_{1,2}(\mu)$, we adjusted the reflection peak widths $\Delta\omega_{1,2}(\mu)$ and the reflection peak heights $R_{1,2}(\mu)$ to obtain an optimal fit of the diffusion model [Eq. (3)] with internal reflection [Eq. (5)] to the data. We expect the parameter functions $R_{1,2}(\mu)$ and $\Delta\omega_{1,2}$ to vary smoothly with angle and we approximate them using cubic polynomials in μ. The polynomial coefficients are determined by a nonlinear least-squares minimization algorithm to fit Eq. (3) to the data.

B. Escape Functions and Band Structure

Here we discuss the agreement between the data and the model outlined above and the angle dependence of the fitted lowest-order peak reflectivity. In Section 6 we review the frequency dependence of the extrapolation length ratio specified by the fitted $R_D(\omega;\mu)$ through Eq. (1).

In Fig. 5(b) both the fit to the data in Fig. 5(a) and the lowest six calculated bands are displayed. The average difference between the measured and theoretical escape function is better than 5–10%. The excellent agreement between the data and the model [Eqs. (3) and (5)] is striking, given the assumptions in the model for the internal reflection coefficient, the empirical nature of the expression [Eq. (3)] for the escape function, and the limitations on the validity of diffusion theory imposed by the modest optical sample thickness ($2 < L/\ell < 10$).

Figure 5(b) clearly demonstrates that, for a quantitative understanding of the angle-resolved diffuse transmission, the band structure is useful but *not sufficient*. Although the first diffraction order at near-normal incidence in the band structure evidently corresponds to

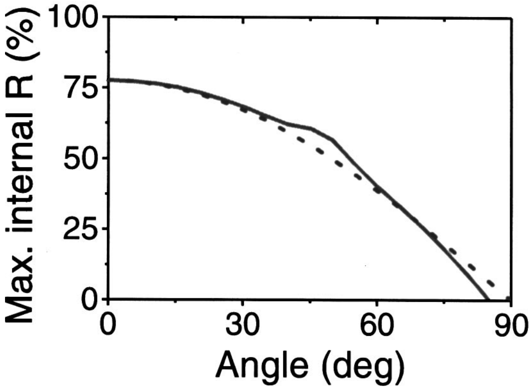

Fig. 6. Solid curve is the fitted peak internal reflection coefficient of the lowest-order stop band versus exit angle α pertaining to the fit [Fig. 5(b)] to the experimental data shown in Figs. 3, 4, and 5(a). The peak internal reflection coefficient typically decreases with $\cos(\alpha)$ (dashed curve).

the attenuation band in the diffuse transmission, the enhanced transmission probability for wave vectors outside a stop band cannot be explained from the dispersion relation alone. The extrapolation length ratio is the essential parameter determining the redistribution of intensity over exit directions.

It is interesting to monitor the fitted internal reflection peak height and the fitted widths of the two photonic stop gaps. We find that the fitted width $\Delta\omega_1$ of the lowest-frequency stop gap at a normal exit angle is 430 cm^{-1}, corresponding to a FWHM of 1000 cm^{-1}. This width is in good agreement with the width of the L gap determined in reflectivity experiments.[44] Although the width $\Delta\omega_2$ of the higher gap stays nearly constant at 660 cm^{-1}, the fitted width of the lowest gap increases approximately quadratically with increasing exit angle α to $\approx$770 cm^{-1} at a grazing exit angle. The magnitude and frequency dependence of the fitted widths are in agreement with the calculated band structure. Of special interest is the fitted internal reflection coefficient $R_1(\mu)$ of the lowest stop gap as a function of the photon escape angle α. As shown in Fig. 6 for the fit to the experimental data in Fig. 5(a), we find a decrease of the reflection coefficient of the lowest gap with increasing angle, which follows a cosine behavior over a large angular range.

This supports an earlier proposition[41] stating that the stop gap depth for $\alpha=0°$ in luminescence spectra, i.e., with an internal source of diffuse light, is determined by the ratio of the Bragg attenuation length and the transport mean free path ℓ. Briefly, diffuse photons emanating from a depth $z<\ell$ from the crystal–air interface propagate ballistically to the interface, but can be redirected to the detector by scattering by defects. Since ℓ is larger than the Bragg attenuation length ($\ell\approx 5\times L_B$), light scattered at $z<L_B$ is hardly Bragg attenuated, and light scattered at a depth $L_B<z<\ell$ develops a stop band (compare with Fig. 1). The stop band minimum for $\alpha=0°$ is therefore estimated as $1-R\approx 1-L_B/\ell$. This geometric argument can be generalized by noting that, for larger exit angles α, the path length to the crystal–air interface increases with $\cos\alpha$. This increases the probability of being scattered at $z<L_B$, reducing the internal reflection coefficient to $1-R\approx 1-L_B\cos\alpha/\ell$, in agreement with Fig. 6. We conclude that the mechanism of diffusion and internal reflection proposed for the angular redistribution of fluorescence from sources inside strongly interacting photonic crystals[41] is confirmed by the present results and analysis.

6. EXTRAPOLATION LENGTH AND TOTAL TRANSMISSION

We use the extrapolation length ratio that results from the model of the measured escape function to interpret the total transmission $T(\omega;\gamma)$ of the inverse opals in terms of the transport mean free path. First we present total diffuse transmission spectra obtained in the experiment in Subsection 6.A. In Subsection 6.B we analyze the frequency dependence of the extrapolation length ratio and discuss total transmission corrected for internal reflections.

A. Total Transmission

The total transmission of a sample with $a=930$ nm is shown in Fig. 7 as a function of frequency for incidence angles $\gamma=0°$, 15°, and 30°. The most apparent features are (i) the occurrence of a band of reduced total transmission that shifts from 8100 cm^{-1} to higher frequencies with increasing angle of incidence and (ii) a decrease of the total transmission with increasing frequency visible in all three traces. For each angle, the center frequency of the band of reduced transmission coincides with the photonic stop band obtained from angle-resolved reflectivity and with the stop band in the escape function. The stop band center frequency is inversely proportional to the lattice parameter, as demonstrated by the blueshifted spectrum for a sample with $a=800$ nm in Fig. 7. As less light enters the sample for wave vectors matching the Bragg reflection condition, the diffuse intensity injected into the sample is reduced in a frequency region matching the stop band for the incident direction. Since this reduction of the total transmission is caused by the reflectivity of the front surface $[1-R_{\text{front}}(\omega;\gamma)]$ in Eq. (2), the stop band width in

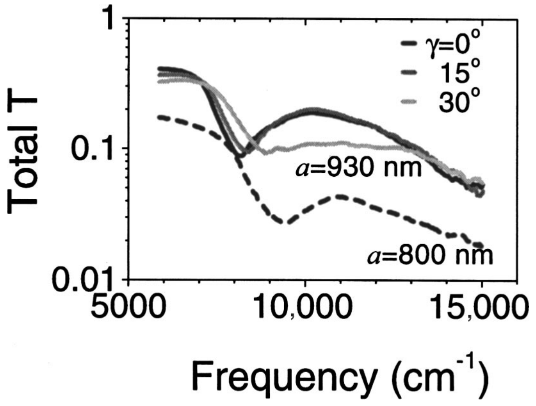

Fig. 7. Total diffuse transmission as a function of optical frequency for a sample with lattice parameter $a=930$ nm for incidence angles $\gamma=0°,15°,30°$ (solid black, gray, and light gray curves, respectively). For a sample with $a=800$ nm, the stop gap at $\gamma=0°$ (L gap) is shifted to a higher frequency (dashed curve).

the total transmission measurement is larger than the photonic width because of the angular spread of the incident beam.

The stop band depth in total transmission is limited by the external reflectivity R_{front}, which amounts to 50–70% for a wide beam spanning many domains. The stop band minimum of 0.09 at $\gamma = 0°$ in the total transmission is indeed only two to three times less than the value just outside the stop band of roughly 0.3. This should be contrasted to the typical attenuation of several decades for stop bands in characteristic "coherent transmission" measurements, in which the intensity transmitted along the incident beam is monitored. As the coherent transmission decays exponentially with ℓ / L, such measurements are feasible only in thin (i.e., small L)[15] or near-index-matched (i.e., large ℓ)[22] photonic crystals. The stop gap in coherent transmission is determined by diffraction from all the differently oriented crystallites encountered along the trajectory of the forward beam. The cumulative effect of all crystallites in the bulk causes a stop gap with high attenuation and a width larger than the intrinsic photonic width.[18] This broadening is not only limited by the angular spread of the incident beam, however, but is mainly caused by misaligned and strained crystallites.[50]

The decrease of the total transmission with increasing frequency is caused by a decrease of the mean free path ℓ due to an increasing scattering strength of defects for larger frequencies. We recognize two regimes in the total transmission, dependent on the magnitude of the mean free path. Below $\omega = 7200\ \text{cm}^{-1}$, the total transmission of ~ 0.3 indicates that the sample thickness of $\sim 200\ \mu\text{m}$ is at most a few transport mean free paths ($\ell \approx 60\ \mu\text{m}$). In this regime the sample is not truly multiple scattering, causing deviations of the diffusion law [Eq. (2)] that relates ℓ to total transmission. For higher frequencies we find a steeper decrease of the total transmission to ~ 0.05 at $\omega = 15{,}000\ \text{cm}^{-1}$. In this frequency range of $\omega \geqslant 7200\ \text{cm}^{-1}$, the mean free path is sufficiently small compared to the sample thickness, so we expect the Ohmic diffuse transmission law [Eq. (2)] to hold. As the lowest Bragg diffraction overlaps with this frequency range, however, the analysis of total transmission in terms of the mean free path is complicated by the frequency dependence of the extrapolation length ratio.

B. Extrapolation Length Ratio and Scattering Strength

In the lower panel of Fig. 8 we present the extrapolation length ratio z_e / ℓ as a function of frequency, obtained from the model shown in Fig. 5. In the low-frequency limit, the extrapolation length ratio equals 2/3, as there are no internal reflections. As the optical frequency reaches the L gap, the extrapolation length ratio grows to a maximum of nearly 1.8. This maximum is reached at the blue edge of the L gap, where the largest fraction of solid angle is covered by stop gaps.[9] The avoided crossing of two stop bands at $\alpha \geqslant 30°$ close to the same frequency enlarges the range of internal reflection, leading to a maximum angle-averaged reflectivity $\bar{R}_D(\omega)$, as can be seen from Eq. (1). For higher frequencies $\omega > 9500\ \text{cm}^{-1}$, the extrapolation length ratio diminishes as the range of internally reflected angles decreases. Although the qualitative behavior of the extrapolation length ratio can be explained by the band structure, the numerical value of the maximum and details of the functional dependence are determined by, e.g., the depth of the stop gaps involved.

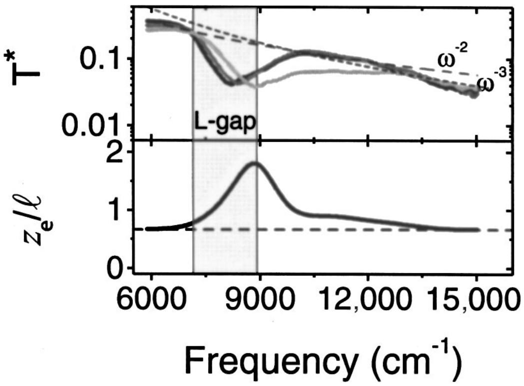

Fig. 8. $\tau_e = z_e / \ell$ pertaining to the fit to the data in Fig. 5. Upper panel: $T^* = T / (1 + \tau_e [1 - 2T])$ for incidence angles $\gamma = 0°, 15°, 30°$ (black, dark gray, and light gray curves, respectively). Dashed curves represent the power laws ω^{-3} (short dashes) and ω^{-2} (long dashes).

We now discuss the scaling behavior of the decrease of the total transmission with increasing frequency. From Eq. (2) it is clear that, for frequencies outside a stop gap for the incident direction (for which $R_{\text{front}} = 0$) the inverse optical thickness ℓ / L can be expressed in terms of T and $\tau_e = z_e / \ell$ as $\ell / L = T / (1 + \tau_e - 2\tau_e T)$. Using the extrapolation length ratio $\tau_e(\omega)$ plotted in Fig. 8, we extract $T^* = T / (1 + \tau_e - 2\tau_e T)$ from the total transmission spectra presented in Fig. 7. The value $T^* \sim 0.1$ at frequencies around $10{,}000\ \text{cm}^{-1}$ is typical of a mean free path of $\ell \approx 20\ \mu\text{m}$, given the estimated sample thickness $L \sim 200\ \mu\text{m}$. Although this value of ℓ agrees with enhanced backscattering experiments on other samples,[24] we focus on the behavior of T^* with frequency, as the thickness L of the samples is not accurately known. We have recently shown, however, that if many such uncalibrated total transmission spectra for different samples are combined and matched to absolute measurements of ℓ for a few frequencies, the magnitude of the mean free path can be determined over a wide frequency range.[25] As T^* equals ℓ / L for frequencies outside a stop gap in total transmission, one might expect a ω^{-4} law typical for the scattering strength of particles much smaller than the wavelength, as reported for opals.[22] Instead we find a decrease of ℓ / L that appears faster than ω^{-2} and slower than ω^{-3} behavior. This observation also holds for the samples with $a = 930$, 900, and 800 nm and was reproduced on samples with much smaller lattice parameters $a = 690$ and 500 nm. For the latter samples, the frequencies in the range of the experiment remain below the L gap, i.e., the long-wavelength regime. Although the frequency dependence of ℓ remains partly obscured because of the stop bands in total transmission, the scattering does not increase as fast as Rayleigh's ω^4 law predicts. This behavior is consistent with a scattering mechanism described in Ref. 25, which quantitatively explains the increase of scattering strength as ω^2 for all 3D photonic crystals. According to this model, the size polydispersity and small rms displacements of each building block are the dominant scattering mechanisms rather than, e.g., missing spheres, stacking faults, and grain boundaries. The fabrication of periodic structures with template-assisted self-assembly,[11,42,51–53] lithographic,[54,55] and layer-by-layer microfabrication methods[56] all involve displacements, roughness, and polydispersity of the same magnitude. Hence the scattering losses are comparable in all the strongly photonic state-of-the-art structures. Consequently, the pursuit of large ($L > 1$ mm) photonic crystals that are so-called defect free, i.e., with as low a density of point defects as possible,[57] is not warranted. A second, favorable consequence of the frequency scaling concerns the photonic bandgap of fcc crystals that is anticipated in the range of second-order diffraction.[49,58] Since the ω^{-2} to ω^{-3} decrease of the mean free path is slower than the earlier expected Rayleigh behavior, the scattering losses will be less at the high frequencies where the bandgap is expected.

7. CONCLUSION

We have presented frequency-resolved measurements of the angular distribution of diffusely transmitted light from strongly interacting photonic crystals. We find a drastic frequency-dependent angular redistribution of diffusely transmitted light due to internal Bragg reflection. Although the ranges of strong internal reflection are governed by gaps in the dispersion relation, it is imperative for accurate modeling to take into account the redistribution into angles not contained in a stop gap. The relevant parameter, i.e., the extrapolation length ratio, cannot be derived from the band structure, but rather from a diffusion model.

We have presented the first model combining diffusion and the photonic internal reflection due to the band structure. The extrapolation length ratio that we calculate has a broader relevance in interpreting standard experiments such as enhanced backscattering or total transmission aimed at determining the transport mean free path in the frequency range of photonic stop gaps. Application to the total transmission of strongly interacting photonic crystals reveals a mean free path decreasing from ~ 60 to ~ 10 μm as the frequency increases from below the first stop gap to just below the second-order Bragg reflection. This decrease is surprisingly slower than ω^{-4}, indicating that polydispersity, roughness, and site displacements of photonic building blocks form the dominant scattering mechanism. Our results are especially important for interpreting experiments on light that is emitted by light sources inside photonic crystals, which is one of the driving forces in the field of photonics.

ACKNOWLEDGMENTS

We thank Ad Lagendijk for helpful and encouraging discussions, Lydia Bechger for sample preparation, Gerard Wegdam for facilitating experiments at the van der Waals-Zeeman Institute (University of Amsterdam), and Peter Lodahl for carefully reading the manuscript. This work is part of the research program of the Stichting voor Fundamenteel Onderzoek der Materie, which is financially supported by the Nederlandse Organisatie voor Wetenschappelijk Onderzoek.

Femius Koenderink's current address is Nano-Optics Group, Laboratory for Physical Chemistry, Swiss Federal Institute of Technology, Zürich (ETH), Switzerland. His e-mail address is femius.koenderink@phys.chem.ethz.ch. Willem Vos can be reached by e-mail at W.L.Vos@utwente.nl and on the web at www.photonicbandgaps.com.

REFERENCES

1. E. Yablonovitch, "Inhibited spontaneous emission in solid-state physics and electronics," Phys. Rev. Lett. **58**, 2059–2062 (1987).
2. S. John, "Strong localization of photons in certain disordered dielectric superlattices," Phys. Rev. Lett. **58**, 2486–2489 (1987).
3. C. M. Soukoulis, ed., *Photonic Crystals and Light Localization in the 21st Century* (Kluwer Academic, Dordrecht, The Netherlands, 2001).
4. O. J. Painter, R. K. Lee, A. Scherer, A. Yariv, J. D. O'Brien, P. D. Dapkus, and I. Kim, "Two-dimensional photonic band-gap defect mode laser," Science **284**, 1819–1821 (1999).
5. S. J. McNab, N. Moll, and Y. A. Vlasov, "Ultra-low loss photonic integrated circuit with membrane-type photonic crystal waveguides," Opt. Express **11**, 2927–2939 (2003), http://www.opticsexpress.org.
6. H. Kosaka, T. Kawashima, A. Tomita, M. Notomi, T. Tamamura, T. Sato, and S. Kawakami, "Superprism phenomena in photonic crystals," Phys. Rev. B **58**, R10096–R10099 (1998).
7. A. F. Koenderink, P. M. Johnson, J. F. Galisteo Lopez, and W. L. Vos, "Three-dimensional photonic crystals as a cage for light," C. R. Phys. **3**, 65–77 (2002).
8. C. Lopez, "Recent review on fabrication of photonic crystals," Adv. Mater. (Weinheim, Ger.) **15**, 1679–1704 (2003).
9. M. S. Thijssen, R. Sprik, J. E. G. J. Wijnhoven, M. Megens, T. Narayanan, A. Lagendijk, and W. L. Vos, "Inhibited light propagation and broadband reflection in photonic air-sphere crystals," Phys. Rev. Lett. **83**, 2730–2733 (1999).
10. S. Noda, K. Tomoda, N. Yamamoto, and A. Chutinan, "Full three-dimensional photonic bandgap crystals at near-infrared wavelengths," Science **289**, 604–606 (2000).
11. Y. A. Vlasov, X. Z. Bo, J. C. Sturm, and D. J. Norris, "On-chip natural assembly of silicon photonic bandgap crystals," Nature (London) **414**, 289–293 (2001).
12. A. F. Koenderink, L. Bechger, H. P. Schriemer, A. Lagendijk, and W. L. Vos, "Broadband fivefold reduction of vacuum fluctuations probed by dyes in photonic crystals," Phys. Rev. Lett. **88**, 143903 (2002).
13. P. Lodahl, A. F. van Driel, I. S. Nikolaev, A. Irman, K. Overgaag, D. Vanmaekelbergh, and W. L. Vos, "Controlling the dynamics of spontaneous emission from quantum dots by photonic crystals," Nature (London) **430**, 654–657 (2004).
14. N. W. Ashcroft and N. D. Mermin, *Solid State Physics* (Holt, Rinehard & Winston, New York, 1976), pp. 616–620.
15. J. F. Bertone, P. Jiang, K. S. Hwang, D. M. Mittleman, and V. L. Colvin, "Thickness dependence of the optical properties of ordered silica-air and air-polymer photonic crystals," Phys. Rev. Lett. **83**, 300–303 (1999).
16. Y. A. Vlasov, V. N. Astratov, A. V. Baryshev, A. A. Kaplyanskii, O. Z. Karimov, and M. F. Limonov, "Manifestation of intrinsic defects in optical properties of self-organized opal photonic crystal," Phys. Rev. E **61**, 5784–5793 (2000).
17. V. N. Astratov, A. M. Adawi, S. Fricker, M. S. Skolnick, D. M. Whittaker, and P. N. Pusey, "Interplay of order and disorder in the optical properties of opal photonic crystal," Phys. Rev. B **66**, 165215 (2002).

18. M. Megens, J. E. G. J. Wijnhoven, A. Lagendijk, and W. L. Vos, "Light sources inside photonic crystals," J. Opt. Soc. Am. B **16**, 1403–1408 (1999).
19. P. A. Lee and T. V. Ramakrishnan, "Disordered electronic systems," Rev. Mod. Phys. **57**, 287–337 (1985).
20. P. Sheng, *Introduction to Wave Scattering, Localization, and Mesoscopic Phenomena* (Academic, New York, 1995).
21. K. Busch and C. M. Soukoulis, "Energy-density CPA: a new effective medium theory for classical waves," Physica B **296**, 56–61 (2001).
22. Y. A. Vlasov, M. A. Kaliteevski, and V. V. Nikolaev, "Different regimes of light localization in a disordered photonic crystal," Phys. Rev. B **60**, 1555–1562 (1999).
23. J. Huang, N. Eradat, M. E. Raikh, Z. V. Vardeny, A. A. Zakhidov, and R. H. Baughman, "Anomalous coherent backscattering of light from opal photonic crystals," Phys. Rev. Lett. **86**, 4815–4818 (2001).
24. A. F. Koenderink, M. Megens, G. van Soest, W. L. Vos, and A. Lagendijk, "Enhanced backscattering from photonic crystals," Phys. Lett. A **268**, 104–111 (2000).
25. A. F. Koenderink, A. Lagendijk, and W. L. Vos, "Optical loss due to intrinsic structural variations in photonic crystals," preprint, http://arxiv.org/abs/physics/0406052 (2004).
26. Z. Y. Li and Z. Q. Zhang, "Fragility of photonic band gaps in inverse-opal photonic crystals," Phys. Rev. B **62**, 1516–1519 (2000).
27. Z. Y. Li, X. D. Zhang, and Z. Q. Zhang, "Disordered photonic crystals understood by a perturbation formalism," Phys. Rev. B **61**, 15738–15748 (2000).
28. M. M. Sigalas, C. M. Soukoulis, C. T. Chan, R. Biswas, and K. M. Ho, "Effect of disorder on photonic band gaps," Phys. Rev. B **59**, 12767–12770 (1999).
29. A. F. Koenderink and W. L. Vos, "Light exiting real photonic band gap crystals is diffuse and strongly directional," Phys. Rev. Lett. **91**, 213902 (2003).
30. L. Bechger, P. Lodahl, and W. L. Vos, "Directional fluorescence spectra of laser dye in opal and inverse opal photonic crystals," J. Phys. Chem. B (to be published).
31. I. S. Nikolaev, P. Lodahl, and W. L. Vos, "Quantitative analysis of directional spontaneous emission spectra from light sources in photonic crystals," preprint, http://arxiv.org/abs/physics/0410056 (2004).
32. J. F. Galisteo Lòpez and W. L. Vos, "Angle resolved reflectivity of single-domain photonic crystals: effects of disorder," Phys. Rev. E **66**, 036616 (2002).
33. A. Ishimaru, *Wave Propagation and Scattering in Random Media* (Academic, New York, 1978).
34. A. Lagendijk, R. Vreeker, and P. de Vries, "Influence of internal reflection on diffusive transport in strongly scattering media," Phys. Lett. A **136**, 81–88 (1989).
35. J. X. Zhu, D. J. Pine, and D. A. Weitz, "Internal reflection of diffusive light in random media," Phys. Rev. A **44**, 3948–3959 (1991).
36. M. U. Vera and D. J. Durian, "Angular distribution of diffusely transmitted light," Phys. Rev. E **53**, 3215–3224 (1996).
37. D. J. Durian, "Influence of boundary reflection and refraction on diffusive photon transport," Phys. Rev. E **50**, 857–866 (1994).
38. J. Gómez Rivas, R. Sprik, A. Lagendijk, L. D. Noordam, and C. W. Rella, "Static and dynamic transport of light close to the Anderson localization transition," Phys. Rev. E **63**, 046613 (2001).
39. F. J. P. Schuurmans, D. Vanmaekelbergh, J. van de Lagemaat, and A. Lagendijk, "Strongly photonic macroporous gallium phosphide networks," Science **284**, 141–143 (1999).
40. M. Notomi, "Theory of light propagation in strongly modulated photonic crystals: refraction like behavior in the vicinity of the photonic band gap," Phys. Rev. B **62**, 10696–10705 (2000).
41. H. P. Schriemer, H. M. van Driel, A. F. Koenderink, and W. L. Vos, "Modified spontaneous emission spectra of laser dye in inverse opal photonic crystals," Phys. Rev. A **63**, 011801 (2001).
42. J. E. G. J. Wijnhoven, L. Bechger, and W. L. Vos, "Fabrication and characterization of large macroporous photonic crystals in titania," Chem. Mater. **13**, 4486–4499 (2001).
43. M. Megens and W. L. Vos, "Particle excursions in colloidal crystals," Phys. Rev. Lett. **86**, 4855–4858 (2001).
44. H. M. van Driel and W. L. Vos, "Multiple Bragg wave coupling in photonic band-gap crystals," Phys. Rev. B **62**, 9872–9875 (2000).
45. S. G. Romanov, T. Maka, C. M. S. Torres, M. Muller, R. Zentel, D. Cassagne, J. Manzanares-Martinez, and C. Jouanin, "Diffraction of light from thin-film polymethylmethacrylate opaline photonic crystals," Phys. Rev. E **63**, 056603 (2001).
46. T. Yoshiyama and I. Sogami, "Kossel line analysis on colloidal crystals in semidilute aqueous solutions," Phys. Rev. Lett. **53**, 2153–2156 (1984).
47. T. Yoshiyama and I. Sogami, "Kossel images as direct manifestations of the gap structure of the dispersion surface for colloidal crystals," Phys. Rev. Lett. **56**, 1609–1612 (1986).
48. Ì. Ì. Tarhan and G. H. Watson, "Photonic band structure of fcc colloidal crystals," Phys. Rev. Lett. **76**, 315–319 (1996).
49. W. L. Vos and H. M. van Driel, "Higher order Bragg diffraction by strongly photonic fcc crystals: onset of a photonic bandgap," Phys. Lett. A **272**, 101–106 (2000).
50. W. L. Vos, M. Megens, C. M. van Kats, and P. Bösecke, "Transmission and diffraction by photonic colloidal crystals," J. Phys.: Condens. Matter **8**, 9503–9507 (1996).
51. J. E. G. J. Wijnhoven and W. L. Vos, "Preparation of photonic crystals made of air spheres in titania," Science **281**, 802–804 (1998).
52. A. Blanco, E. Chomski, S. Grabtchak, M. Ibisate, S. John, S. W. Leonard, C. Lopez, F. Meseguer, H. Miguez, J. P. Mondia, G. A. Ozin, O. Toader, and H. M. van Driel, "Large-scale synthesis of a silicon photonic crystal with a complete three-dimensional bandgap near 1.5 micrometers," Nature (London) **405**, 437–440 (2000).
53. O. D. Velev and E. W. Kaler, "Structured porous materials via colloidal crystal templating: from inorganic oxides to metals," Adv. Mater. (Weinheim, Ger.) **12**, 531–534 (2000).
54. T. Baba and N. Fukaya, "Light propagation characteristics of defect waveguides in a photonic crystal slab," in Ref. 3, pp. 105–116 (2000). In pioneering work to quantify propagation losses in state-of-the-art silicon-on-insulator 2D photonic crystals, the authors quote an airhole nonuniformity of <4%.
55. M. Notomi, K. Yamada, A. Shinya, J. Takahashi, C. Takahashi, and I. Yokohama, "Extremely large group-velocity dispersion of line defect waveguides in photonic crystal slabs," Phys. Rev. Lett. **87**, 253902 (2001). The authors report a resolution of <5% in diameter and <1% in distance between airholes in Si photonic crystal slabs.
56. S. Ogawa, K. Tomoda, and S. Noda, "Effects of structural fluctuations on three-dimensional photonic crystals operating at near infrared wavelengths," J. Appl. Phys. **91**, 513–515 (2002). The authors report alignment errors less than 7% relative to the wood pile periodicity for optimal strongly photonic GaAs layer-by-layer crystals operating at a 1.2-μm wavelength.
57. R. F. Service, "Building better photonic crystals," Science **295**, 2399 (2002).
58. K. Busch and S. John, "Photonic band gap formation in certain self-organizing systems," Phys. Rev. E **58**, 3896–3908 (1998).